Electronic Supplementary Material (ESI) for Chemical Science.


# Supporting Information

# Unraveling the Effect of Defects, Domain Size, and Chemical Doping on Photophysics and Charge Transport in Covalent Organic Frameworks

Raja Ghosh[*,†] and Francesco Paesani[*,†,‡,¶]

†*Department of Chemistry and Biochemistry, University of California San Diego, La Jolla, California 92093, United States*

‡*Materials Science and Engineering, University of California San Diego, La Jolla, California 92093, United States*

¶*San Diego Supercomputer Center, University of California San Diego, La Jolla, California 92093, United States*

E-mail: raghosh@ucsd.edu; fpaesani@ucsd.edu

# 1 Theoretical Model

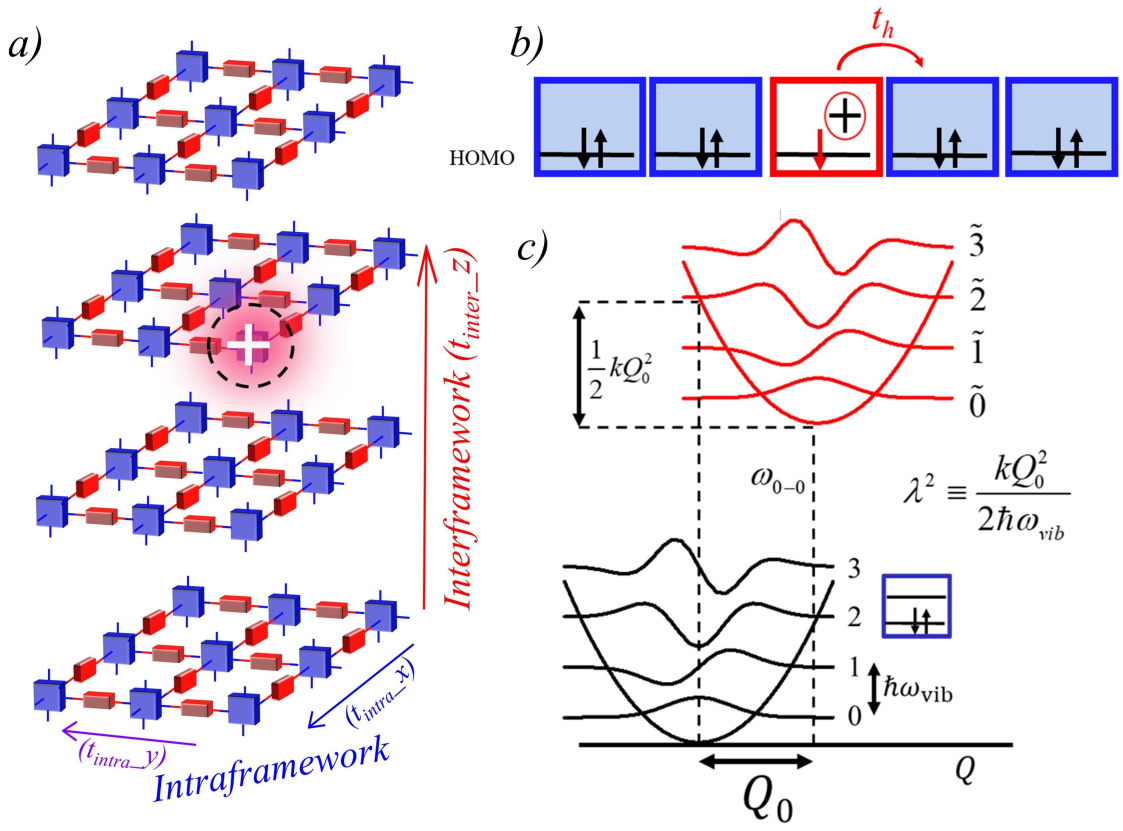


Figure S1: (a) A representative 5×5×4 tetrgaonal COF structure highlighting the important electronic interactions. (b) Schematic showing coupled units hosting a positively charged "hole" polaron. (c). Nuclear potential wells corresponding to the aromatic-quinoidal stretching mode, Q, in the ground and excited electronic states for each isolated molecular unit.

We introduce a three dimensional Holstein model for polarons for our analysis of the mid-IR absorption spectrum of COFs in the presence (or absence) of chemical dopants. A simplified 5×5×4 COF structure highlighting the important electronic interactions is shown in Fig. S1a. The COF 2D plane is taken to be along the x and y axes respectively while the 2D layers are $\pi$-stacked along the z-axis. Every unit in the three dimensional framework is identified by a coordinate (m,n,o). Our treatment of polarons in 2D-COFs is coarse-grained, retaining the local HOMO of each molecular unit as depicted in Fig. S1b. A polaron/hole on any site is a half-filled HOMO, which is coupled to the neighboring units in the 2D x-y plane via the charge transfer (CT) integrals, $t_{intra-x}$ and $t_{intra-y}$ respectively. Similarly, inter-

framework coupling via through space $\pi$-$\pi$ interactions, which arises from the wave function overlap between the HOMOs of neighboring units on adjacent layers, is governed by $t_{inter-z}$. Hence, vibronically mediated electronic coupling induces three dimensional delocalization of the hole over the entire 3D framework. The creation of a (hole)-polaron on a particular site is accompanied by significant nuclear relaxation along the dominant aromatic-quinoidal stretching coordinate which is responsible for the pronounced vibronic progression in the UV-vis spectrum of most conjugated organic materials.[1–3] The associated vibrational frequency, $\omega_{vib}$, is approximately 0.17 $eV/\hbar$ with a Huang-Rhys factor, $\lambda^2$, of approximately one. In order to model chemically doped COF films, we also include the Coulomb interaction between the dopant counter-anion and the hole. In the vector subspace containing a single hole and one counter-anion within a N×N×N disordered framework, the total Hamiltonian can be written as,[4–8]

$$H_{total} = H_0 + H_{disorder} + H_{coulomb} \tag{1}$$

The first term in the Hamiltonian is the Holstein Hamiltonian and is given by,

$$\begin{aligned} H_0 = &\sum_{m=1}^{N-1}\sum_{n=1}^{N}\sum_{o=1}^{N} t_{intra-x}\{d^{+}_{m+1,n,o}d_{m,n,o} + h.c\} + \sum_{m=1}^{N}\sum_{n=1}^{N-1}\sum_{o=1}^{N} t_{intra-y}\{d^{+}_{m,n+1,o}d_{m,n,o} + h.c\} \\ &+ \sum_{m=1}^{N}\sum_{n=1}^{N}\sum_{o=1}^{N-1} t_{inter-z}\{d^{+}_{m,n,o+1}d_{m,n,o} + h.c\} + \hbar\omega_{vib}\sum_{m=1}^{N}\sum_{o=1}^{N}\sum_{n=1}^{N} b^{+}_{m,n,o}b_{m,n,o} \\ &+ \hbar\omega_{vib}\sum_{m=1}^{N}\sum_{n=1}^{N}\sum_{o=1}^{N}\{\lambda(b^{+}_{m,n,o} + b_{m,n,o}) + \lambda^2\}d^{+}_{m,n,o}d_{m,n,o} \end{aligned} \tag{2}$$

The first three terms in $H_0$ represents the local hole's kinetic energy and $\hbar$ is taken to be 1. The operators $d^{+}_{m,n,o}$ and $d_{m,n,o}$ respectively create and annihilate a hole on the $m^{th}, n^{th}, o^{th}$ unit in the 3D framework. The last three terms in $H_0$ account for the local vibronic coupling involving the symmetric aromatic/quinoidal vibration with energy, $\hbar\omega_{vib} =$

$0.17eV$. The operators $b^{+}_{m,n,o}(b_{m,n,o})$ respectively create (annihilate) a vibrational quantum on the $m^{th}, n^{th}, o^{th}$ unit in the framework- the unit at $(m, n, o)$ - within the ground $(S_0)$ potential well. The Huang-Rhys (HR) factor, $\lambda^2$, represents the geometric relaxation energy experienced by a single repeat unit upon oxidation (in units of $\hbar\omega_{vib}$). The HR factor is nonzero whenever the ground and cationic potential wells are shifted relative to each other as shown in Fig.S1b. In all the calculations we have set $\lambda^2$=1. Finally, the Hamiltonian omits a constant term representing the zero-point vibrational energy as well as the on-site polaron energy. As we are interested only in the transition energy between the eigenstates, such terms are not important for our analysis.

The Hamiltonian is modified to include spatially uncorrelated energetic site disorder which arises due to in and out of the plane fluctuations in the torsional angles, chemical defects in the framework, presence of inhomogeneous electric fields etc. Disorder in polymeric materials can be efficiently represented as random fluctuations in the hole's site energy, $\Delta_{m,n,o}$, when the hole is located on the (m,n,o) unit.[9]

$$H_{disorder} = \sum_{m=1}^{N}\sum_{n=1}^{N}\sum_{o=1}^{N} \Delta_{m,n,o} d^{+}_{m,n,o} d_{m,n,o} \tag{3}$$

The deviations, $\Delta_{m,n,o}$, are randomly selected from a Gaussian distribution with standard deviation $\sigma$:

$$P(\Delta_{m,n,o}) = (2\pi\sigma^2)^{-1/2} \exp(-{\Delta^2}_{m,n,o}/2\sigma^2) \tag{4}$$

For undoped COFs, we only consider the first two terms in eq.1. For doped COFs, we also consider the third term, i.e, the electrostatic attraction between the dopant counter-anion and the hole. In the simplest manifestation, the anion is considered to be a negative point charge. Treating the holes as point charges, the Coulomb attraction is given by,

$$H_{coulomb} = \sum_{m=1}^{N}\sum_{n=1}^{N}\sum_{o=1}^{N} \frac{-e^2}{4\pi\epsilon_o\epsilon|\boldsymbol{r_{m,n,o}} - \boldsymbol{r_{anion}}|} d^{+}_{m,n,o} d_{m,n,o} \tag{5}$$

where $r_{m,n,o}$ is the position vector identifying the $m^{th}, n^{th}, o^{th}$ unit while $r_{anion}$ is the position of the dopant anion. Finally, in Eq.5, $\epsilon_0$ is the vacuum permitivity and $\epsilon$ is the (unitless) relative permittivity.

### 1.1 Basis Set

Under the two-particle approximation, the single-hole basis set used to represent $H_0$ in Eq.2 is truncated to include one- and two-particle states, analogous to the one and two-particle states used in treating neutral excitons.[1–3,10] In a single-particle state, denoted as $|m, n, o, \tilde{v}\rangle$, a hole resides on the $m^{th}, n^{th}, o^{th}$ unit in the framework with $\tilde{v}$ vibrational quanta in its shifted $S_+$ potential well. The remaining $N^3 - 1$ monomers are in their vibrationless ground states (filled HOMO with no vibrations in the $S_0$ well). In a two particle state, denoted $|m, n, o, \tilde{v}; m^{'}, n^{'}, o^{'}, v^{'}\rangle$, the monomer $(m, n, o)$ is vibronically excited with $\tilde{v}$ vibrational quanta in its shifted $S_+$ potential well while monomer $(m^{'}, n^{'}, o^{'})$ is vibrationally excited with $v^{'} > 0$ vibrational quanta in the unshifted $S_0$ potential. The remaining $N^3 - 2$ monomers are in their vibrationless ground states. The Holstein Hamiltonina represented in the multiparticle basis set has been very successful in accounting for the spectral properties of molecular aggregates as well as conjugated polymers in the mid-IR[11–18] and UV-Vis regions.[1–3]

## 2 Infrared Absorption and Polaron Coherence

We begin with the expression for the spectrum polarized along the direction $j$

$$A_j(\omega) = \left\langle \sum_{ex} f_j^{ex} W_{LS}[\hbar\omega - (E_{ex} - E_g)] \right\rangle_c \tag{6}$$

Here, the index $j(= x, y, z)$ indicates the polarization, with $x$ and $y$ lying in the COF plane and $z$ is along the stacking (interframework) axis. The sum in Eq.6 is over all the polaron excited states and $< ... >_c$ represents an average over many site-energy disorder

configurations. For our analysis, we typically employ 5000 disorder configurations to obtain spectral convergence. The oscillator strength, $f_j^{ex}$, involving the transition between the polaron ground state, $|\Psi_G>$ and an excited state $|\Psi_{ex}>$ (both of which generally dependent upon the disorder configuration) is given by the oscillator strength,

$$f_j^{ex} = \frac{2m_e}{3e^2\hbar^2}(E_{ex} - E_g)|\langle\psi_G|\hat{\boldsymbol{\mu}}_{\boldsymbol{j}}|\psi_{ex}\rangle|^2 \tag{7}$$

where the vector dipole moment operator in Eq.7 is given by,

$$\hat{\boldsymbol{\mu}} = e\sum_{m,n,o} \boldsymbol{r_{m,n,o}} d^+_{m,n,o} d_{m,n,o} \tag{8}$$

arises from the interaction of the infrared electric field $\boldsymbol{E}$ and the hole, through the interaction term given by,

$$H_{interaction} = \hat{\boldsymbol{\mu}}.\boldsymbol{E} \tag{9}$$

In Eq.8, $r_{m,n,o} = md_{intra}\hat{x} + nd_{intra}\hat{y} + nd_{inter}\hat{y}$ is the position vector locating the $(m, n, o)$ unit, $\hat{x}$, $\hat{y}$, and $\hat{z}$ are the unit vectors along the x, y and z-axes, respectively, and $d_{intra}$ and $d_{inter}$ are the nearest neighbor distances between repeat units in and out of the COF plane respectively. Finally, $W_{LS}$ in Eq.6 is the homogeneous line shape function having a narrow Gaussian with a standard deviation of 0.05 eV, much less than the inhomogeneous width, $\sigma$ = 0.25-0.3 eV that has been used through out this work.

The mid-IR spectrum for the light polarized along each axis (x,y,z) is calculated along with the corresponding polaron coherence function. By quantitatively fitting the measured infrared spectrum, we can extract information about the polaron delocalization lengths, i.e., how far the hole delocalizes along the intraframework (x,y) and interframework(z) directions. We have developed a direct relationship between the mid-IR infrared spectrum and the hole coherence function which is given by,

$$f^{tot}_{intra-x} = \frac{2m_e}{3\hbar^2} d^2_{intra-x} \, |t_{intra-x}| C_P[r = (1,0,0)] \tag{10}$$

$$f^{tot}_{intra-y} = \frac{2m_e}{3\hbar^2} d^2_{intra-y} \, |t_{intra-y}| C_P[r = (0,1,0)] \tag{11}$$

$$f^{tot}_{inter-z} = \frac{2m_e}{3\hbar^2} d^2_{inter-z} \, |t_{inter-z}| C_P[r = (0,0,1)] \tag{12}$$

where $d_{intra-x}(f^{tot}_{intra-x})$, $d_{intra-y}(f^{tot}_{intra-y})$, and $d_{inter-z}(f^{tot}_{inter-z})$ are the nearest neighbor distances(total absorption) along the x,y and z directions respectively. $C_p(r)$ is the three-dimensional coherence function describing hole delocalization and is given by,

$$C_P(r) \equiv \left\langle \langle \Psi_G | \sum_R d^\dagger_{\boldsymbol{R}} d_{\boldsymbol{R}+\boldsymbol{r}} \, |\Psi_G\rangle \right\rangle_C \tag{13}$$

Here, $\boldsymbol{R} = (m, n, o)$ is a dimensionless position vector. When r=0 the coherence reduces to unity, $C_P[(0,0,0)] = 1$, since $\sum_R d^\dagger_{\boldsymbol{R}} d_{\boldsymbol{R}}$ is the operator for the total number of holes, which is taken to be unity.

Eq.'s 10, 11 and 12 show that the total oscillator strength for light polarized along the direction $j(= x, y, z)$ scales as the polaron coherence for a separation of one unit along that direction $(x, y, z)$. Since $C_P[(0,0)]$ is unity independent of disorder, we can begin to appreciate the width of the coherence function in each direction using Eq.s 10, 11 and 12.

These equations therefore provide a direct link between the polarized components of the infrared absorption spectrum and the spatial coherence lengths in the intraframework$(x, y)$ and interframework $(z)$ directions, respectively. In the limit of highly mobile holes along $(x, y, z)$, where $C_P[(1,0,0)]$ $(C_P[(0,1,0)])$ $(C_P[(0,0,1)])$ approaches unity, $f^{tot}_{intra-x}$, $f^{tot}_{intra-y}$, and $f^{tot}_{inter-y}$ are largest, while in the opposite extreme of completely trapped holes, $C_P(r) = C_P[(0,0,0)]\delta_{r,(0,0,0)}$ , the oscillator strength vanishes in either direction. This makes sense, as the polaron transitions induced by infrared excitation involve a moving charge. Fig.1d,f

in the main text show the two extreme scenarios; in the case of an ideal polymer with no site disorder, all the repeat units have the same site energy. As a result, the hole can easily delocalize from the one side of the chain to the other. On the other hand, in the presence of high site disorder, ($\sigma = 0.3$ eV), the hole gets trapped on a site having sufficiently low energy. If a polaron is trapped on a site with sufficiently low energy, it cannot respond to the external electric field and the oscillator strength vanishes. Interestingly, the total oscillator strength for polaron absorption is not conserved with changing disorder, in marked contrast to exciton absorption, where a loss of oscillator strength in one spectral region is compensated by an increase in oscillator strength in another region.[6,8]

# 3 Origin of Peaks A and B

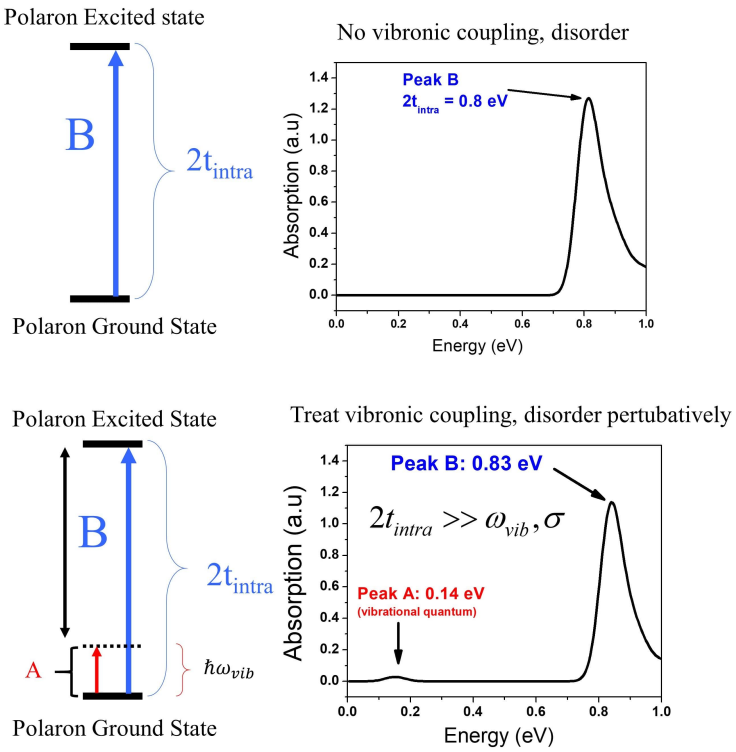


Figure S2: Energy level diagrams for peaks A and B.

The fundamental nature and origin of peaks A and B and the full mathematical deriva-

tions can be found in Refs. 6, 7, 8. In the absence of disorder and vibronic coupling, Peak B in any direction (x,y,z) is an electronic transition from the polaron ground state to the next higher electronic state in that direction. The transition energy along any direction (x,y,z) is determined by the strength of the electronic couplings ($t_{intra-x}$,$t_{intra-y}$,$t_{inter-y}$) along that direction. However, in the presence of disorder and vibronic coupling, the initially dark state, having an energy close to a vibrational quantum of the vinyl stretching mode becomes optically active as it borrows intensity from the dominant peak B, a property that can be understood in terms of Herzberg-Teller coupling mechanism.[6,7] Even in the presence of high site disorder, peak A remains surprisingly narrow while peak B broadens due to perturbation theory and Herzberg-Teller coupling mechanism. The spectral intensity of peak A relative to B is a very important signature of polaron coherence consistent with experimental observations.

## 3.1 Effect of Strong Coulomb Binding on peak B

When the anion ($d_{anion} < 0.4$ nm) is placed in very close proximity to the framework, the strength of Coulomb binding is very strong and overrides disorder induced effects. In this regime of very strong Coulomb binding, even slight changes in the $d_{anion}$ value results in significant blue shift of peak B as shown in Fig.S3b. Strong Coulomb binding between the electron and hole impacts the energy of the nearby repeat unit and isolates it energetically thus resulting in a drastic drop of the polaron ground state energy as shown schematically in Fig.S3a. Hence, the transition energy, from the polaron ground state to the first excited state is quite high in this regime. The ground state energy does not drop drastically when the strength of Coulomb binding is not in the very strong regime ($d_{anion} > 0.4$ nm) or comparable to disorder induced effects.

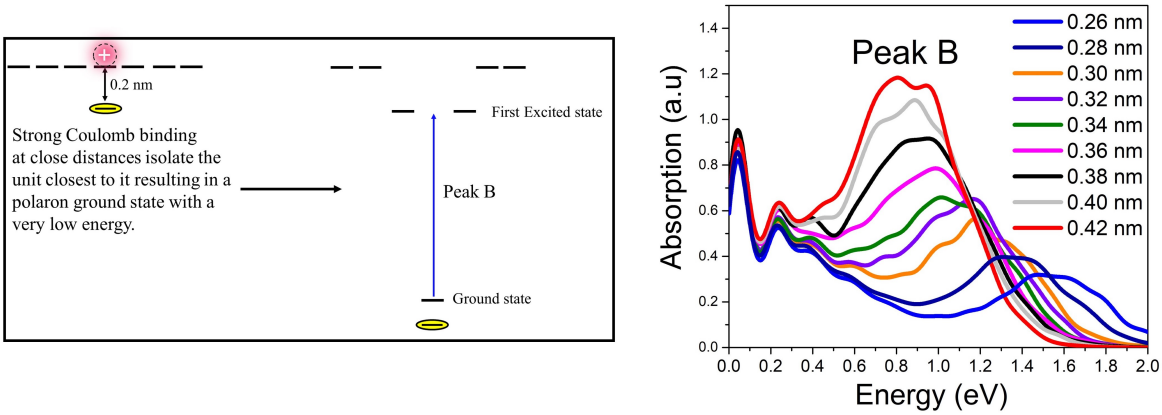


Figure S3: (a) Energy level diagram for peak B. (b) Infrared absorption spectrum as a function of $d_{anion}$ in the very strong Coulomb binding regime.

# 4 Crystalline vs Amorphous Frameworks

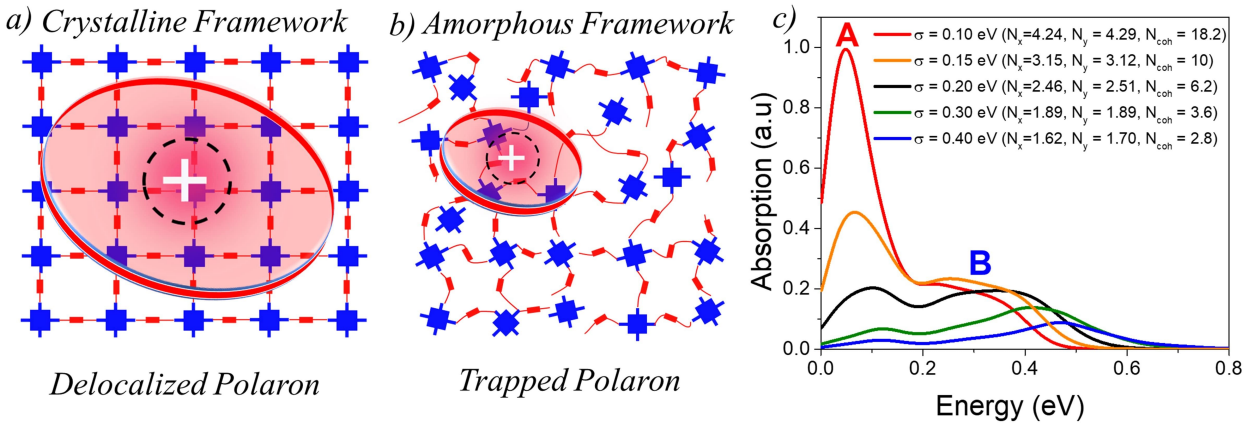


Figure S4: (a-b) Schematic representations of crystalline and amorphous frameworks having delocalized and localized polaron cloud, respectively. (c) Hole absorption spectrum in the mid-IR energy range for a hole in a 9×9 tetragonal COF framework having a pore size of 3 nm for different values of $\sigma$. An average over 5000 disorder configurations was performed for each spectrum to guarantee convergence.

In Fig. S4, we characterize the impact of increasing disorder on the total absorption spectrum for a hole in a 9×9 2D tetragonal lattice. As the disorder width ($\sigma$) is gradually increased, i.e, as we transition from a perfectly crystalline(Fig. S4a) framework to an amorphous framework(Fig. S4b), the spectral signatures follow the same trend as discussed in

the main text. Increasing $\sigma$ results in a dramatic loss of oscillator strength, blue shift and broadening of peak B, reduction of the coherence lengths, and a decrease in A/B peak ratio. The total polaron coherence numbers $N_{coh}$ (approximately equal to the product of $N_x$ and $N_y$) as a function of $\sigma$ are reported in the inset of Fig.S4c.

# 5 Importance of Polarized Measurements on Oriented COF films

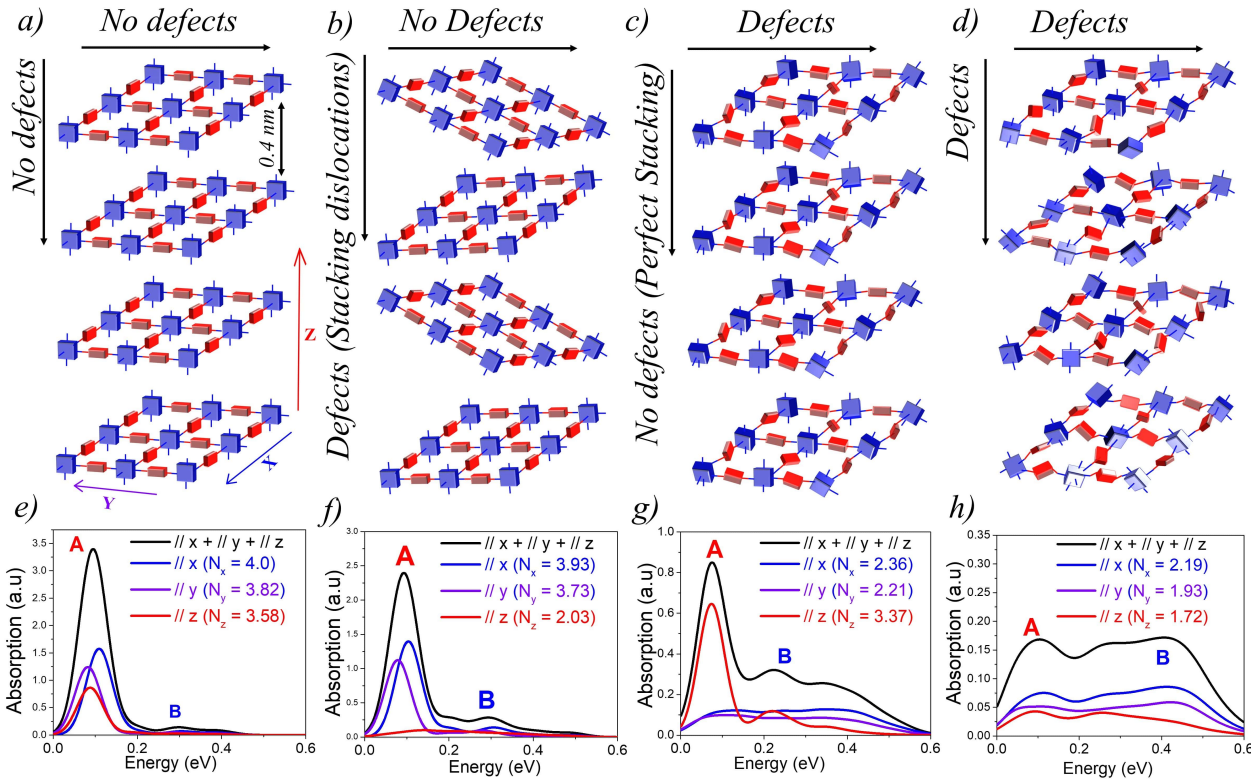


Figure S5: Schematic representations of 5×5×4 frameworks with: (a) perfect 3D order, (b) inter-framework/columnar defects; (c) intra-framework/in-plane defects, and (d) both inter- and intra-framework defects. The associated hole absorption spectra for all the four scenarios are shown in (e-h).

We focus on the impact of electronic defects on the IR spectrum of a 5×5×4 framework hosting a single hole and having a pore size of 3 nm with each repeat unit in the COF plane

separated by a distance of 1.5 nm. The $\pi$ stacking distance between the 2D sheets is taken to be 0.4 nm. In our simulations, we consider four different scenarios as illustrated in Fig. S5(a-d).

In the first scenario, we consider an ideal defect-free 3D framework (Fig.S5a), i.e., all the sites have been given the same random energy. We assume slightly different values of $t_{intra-x}$ (0.25 eV) and $t_{intra-y}$ (0.22 eV) in order to distinguish between the $x$ and $y$ components of the IR spectrum. The disorder width ($\sigma$) in all the four cases is taken to 0.3 eV. The total absorption is shown in black while the $x$, $y$, and $z$ components are shown in blue, violet, and red, respectively. The polaron wavefunction is approximately spread over $N_x = 4.0$, $N_y = 3.82$, and $N_z = 3.58$ units along the $x$, $y$ and $z$ directions, respectively. In the second scenario, we consider only inter-framework columnar disorder(Fig.S5b), with perfect crystalline connectivity and planar arrangement of the monomers within the 2D sheets, and disorder only exists between the molecular stacks. As shown in Fig. S5f, gradual increase in the inter-framework disorder results in the selective attenuation of the spectral intensity and drop in coherence length only along the $z$ component (red) compared to the disorder-free spectrum (Fig. S5e). While the polaron delocalization lengths along $x$ ($N_x = 3.93$) and $y$ ($N_y = 3.73$) remain relatively unchanged, the polaron delocalization lengths along $z$ drops to $N_z = 2.03$ units. In the third scenario, disorder only exists in the 2D sheets and the perfectly aligned stacks are essentially defect-free(Fig.S5c). As shown in Fig.S5g, disorder selectively attenuates the $x$ and $y$ components in the 2D plane, while leaving the $z$ component relatively unchanged. The coherence lengths follow the same trend as shown in the inset of Fig.S5g. Finally, in the fourth and most realistic scenario, we consider both intra- and inter-framework disorder(Fig.S5d) which lead to spectral attenuation of all the three components. The overall polaron cloud further contracts and is now found to approximately spread over $N_x = 2.19$, $N_y = 1.93$, and $N_z = 1.78$ units along the $x$, $y$, and $z$ directions, respectively. Increasing disorder along any axis results in the shrinking of the coherence function, attenuation of the spectral intensity, blue shift and broadening of peak B, and a decrease in the A/B peak

ratio along the same axis. Therefore, the relative position of the peak B maximum and the ratio of the A/B peak directly correlates with polaron coherence. This implies that a small (large) A/B peak ratio along any axis ($x$, $y$, and $z$) can be readily interpreted as a measure of polaron delocalization lengths along that axis, thus highlighting the importance of polarized infrared absorption measurements in 2D organic materials.

# 6 Parameters for Figures

We report the parameters that have been used to simulate the mid-IR absorption spectrum for each figure within the main text as summarized in the tables below.

In Fig. 1(a-c), we have taken a 9×9 tetragonal COF structure, i.e, having 9 and 5 units along x and y directions in the COF plane alternatively and having a pore size of 3 nm. The difference between the three structures is the manner in which disorder has been introduced in the lattice. In long range domains, we have taken a perfectly crystalline lattice, i.e, having no disorder and all the units in the lattice have the same site energy. In medium range domains, within each disorder configuration, every site starting from the $6^{th}$ repeat unit, as illustrated in the main text, is give a site disorder having a random energy, $\Delta_{m,n,o}$, with standard deviation ($\sigma$) of 0.3 eV. Finally, in short range domain, all the units within each disorder configurations are given a site disorder having a random energy, $\Delta_{m,n,o}$, with standard deviation ($\sigma$) of 0.3 eV. In order to obtain absolute spectral convergence, 5000 disorder configurations were done for all the panels. All the remaining parameters are given in the table below.

Table S1: Parameters for the Holstein Hamiltonian in Figure 1g,1h,1i.

| **Figure1(g,h,i)** | **Long/Medium/Short Range Domains** |
|---|---|
| Lattice dimension | 9×9 |
| $t_{intra-x}$ | 0.20 eV |
| $t_{intra-y}$ | 0.20 eV |
| $\sigma$ | 0.3 eV |
| $\Gamma$ | 0.05 eV |
| $\omega_{vib}$ | 1400 $cm^{-1}$ |
| $\lambda^2$ | 1 |

In Fig.2 we show how changing the position of the anion relative to the framework anisotropically impacts the intra- and interframework components of the absorption spectrum and the polaron coherence numbers. Therefore the only changing parameter is the relative position of the anion. All the remaining parameters are given below.

Table S2: Parameters for the Holstein Hamiltonian in Figure 2.

| **Figure2** | **Effect of dopants** |
|---|---|
| Lattice dimension | 3×3×5 |
| $t_{intra-x}$ | 0.14 eV |
| $t_{intra-y}$ | 0.14 eV |
| $t_{inter-z}$ | 0.025 eV |
| $\sigma$ | 0.25eV |
| $\Gamma$ | 0.05 eV |
| $\omega_{vib}$ | 1400 $cm^{-1}$ |
| $\lambda^2$ | 1 |
| $\epsilon_0$ | 2 |

# 7 Comparison to Experiments

The parameters used for all our comparison to experiments is shown in TableS3.

Table S3: Parameters for the Holstein Hamiltonian in Figure 3b,4b,5

| **Figure3b,4b,5** | **Comparison to Experiments** |
|---|---|
| Lattice dimension | 3×3×5 |
| $t_{intra-x}$ | 0.14 eV |
| $t_{intra-y}$ | 0.14 eV |
| $t_{inter-z}$ | 0.025 eV |
| $\sigma$ | 0.25eV |
| $\Gamma$ | 0.05 eV |
| $\omega_{vib}$ | 1400 $cm^{-1}$ |
| $\lambda^2$ | 1 |
| $\epsilon_0$ | 2 |

## 7.1 Transfer Integrals

For our comparison with experimental measurements, we have used the intra-framework and inter-framework nearest neighbor coupling values calculated for prototypical iodine doped COFs.[19] In Ref. 19, the in and out of plane integrals were calculated for a series of doped COF structures having different building blocks and functional groups and most of the calculated values are similar to what we have used for our analysis. In Fig.S6, we report our comparison to experiment with slight variations in the parameters. Keeping all the parameters defining the hamiltonian as shown in TableS3 fixed, the intra-framework coupling was changed to 0.12 eV. The corresponding simulation is shown in Fig.S6a. Even decreasing the intra-framework coupling by half ($t_{intra-x,y} = 0.07$ eV) results in a slightly bad fit (Fig.S6b), in the sense, we do not get the ratio of A/B to agree perfectly with the measured spectrum. However, all our conclusions discussed in the main text remain unchanged. We get similar agreements or slight differences when varying the inter-framework couplings.

## 7.2 Vibronic coupling

Most conjugated organic materials vibrate along the prominent aromatic to quinoidal stretching mode that occurs around 1300-1400 $cm^{-1}$. Keeping all the parameters as shown in Table S3 fixed, we repeated the simulations using 1300 $cm^{-1}$ which gives an equally good fit with

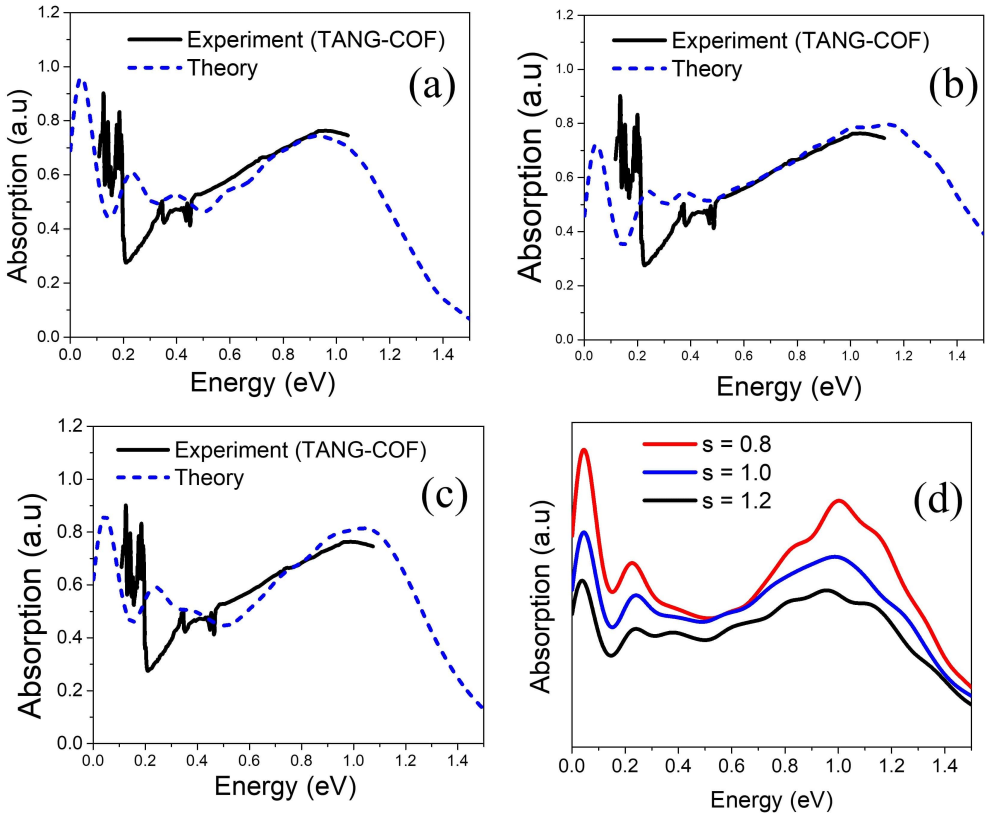


Figure S6: (a) $t_{intra-x,y} = 0.12$ eV. (b) $t_{intra-x,y} = 0.07$ eV. (c) $w_{vib} = 1300$ cm$^{-1}$ (d) Simulated spectrum as a function of HR Factor(s).

the experimental measurement as shown in Fig. S6c.

### 7.2.1 Huang Rhys Factor

The Huang-Rhys (HR) factor ($\lambda^2$) represents the geometric relaxation energy experienced by a single repeat unit in the framework upon oxidation (in units of $\hbar\omega_{vib}$). The HR factor is nonzero whenever the ground and cationic potential wells are shifted relative to each other as shown in Fig. S1b. We have used a HR factor of one for our simulations. In Fig.S6d, we show how the simulations respond to varying $\lambda^2$. Gradually increasing the value of $\lambda^2$ results in a drop in the spectral intensity. However, the most important features relevant for our analysis, i.e., the relative positions of peak A and B and the ratio of peak A/B remain relatively unchanged and our conclusions still hold.

## 7.3 Effect of topology

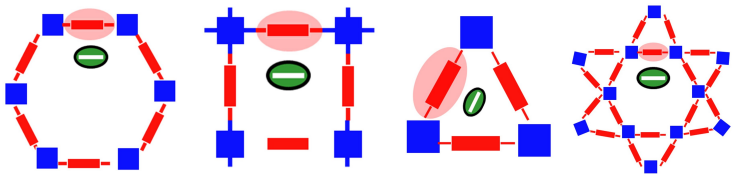

Figure S7: Schematic showing localized polaron wavefuction due to very strong Coulomb binding with the counter-anion that resides in close proximity to the backbone.

Our quantitative comparison with the measured absorption spectrum involves the configuration where the presence of the anion greatly localizes the polaron wavefunction to slightly greater than one unit along the x and z axes. This subspace is inherently present in all COF topologies as shown schematically in Fig. S7. Had we used a different topology (for eg. hexagonal/trigonal/kagome) and kept all the remaining parameters defining the Hamiltonian unchanged (Table. S3), we would still get very similar agreements with the measured absorption spectrum. We anticipate the trigonal arrangement to exhibit slightly different spectral signatures and this will be reported in a forthcoming study. However, none of the comparisons to experiments in this study involve a COF which has a trigonal topology. The effect of topology may become more prominent in the case of unbound holes which, being free to delocalize over the entire framework, can take advantage of the 3D topological arrangement. In such scenarios, the spectrum may slightly vary and the inter- and intra-framework components will be different. Additional experiments and theoretical studies are needed to completely characterize the impact of topology on charge migration in 2D-COFs.

## 7.4 Effect of $d_{anion}$

When the anion is placed at a distance of 0.36 nm from the framework backbone (1.14 nm from the center of the pore, Fig. S8b), the simulated spectrum is in good agreement with experimental measurement (Fig. S8a). However, the anions are not fixed and they are moving around in the COF matrix. Therefore, placing the anion just at one position

is unrealistic and the anion can be present at various locations inside the pore. In our simulations, when we place the counter-anion at distances between 0.30 nm and 0.45 nm from the framework and take the average, the simulated absorption spectrum gives an even better fit as shown in Fig. S8d. Commenting on the precise location of the anion inside the framework is beyond the scope of our theory. However, our analysis shows that the anions preferentially reside at a distance of 0.3 nm -0.45 nm from the framework backbone such that the the polaron wavefunction is greatly localized.

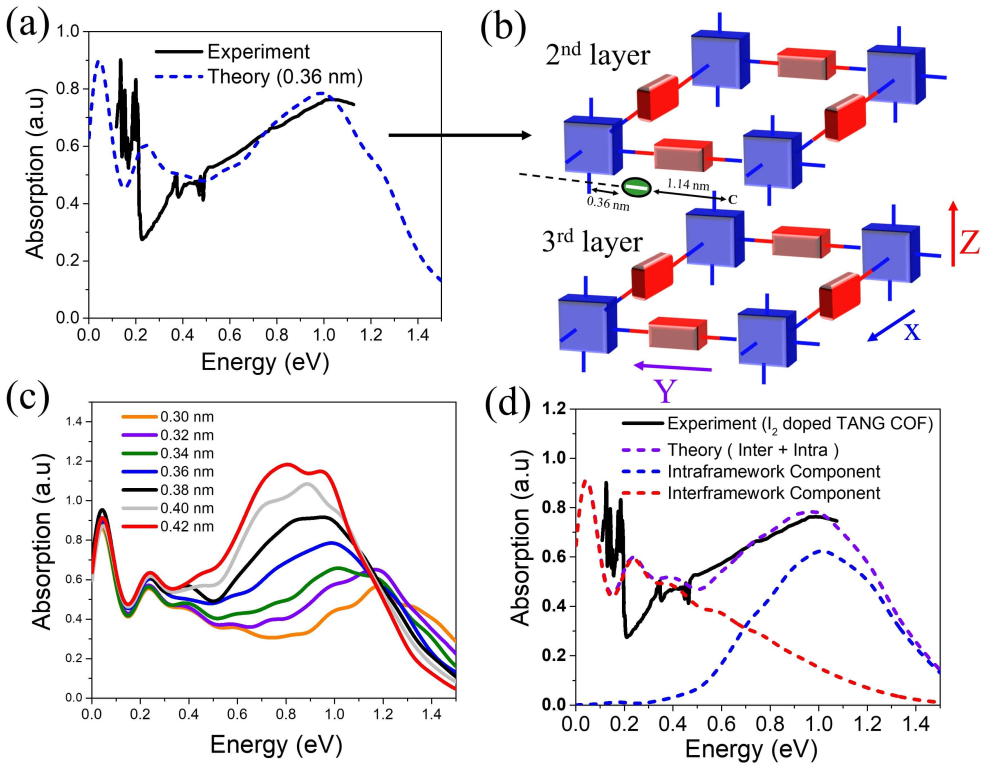


Figure S8: (a) The total absorption spectrum (inter+intra) fitted to the measured spectra of iodine doped TANG-COF using one anion position as illustrated in (b). (b). The anion is positioned between the second and third layer at a distance of 0.36 nm from the framework backbone (x axis) and 1.14 nm from the pore. (c) The total spectrum (inter+intra) for several anion positions. (d) The averaged absoprtion spectrum from different anion positions as shown in (c) quantitatively agrees with the measured spectrum. The inter- and intra-framework components are also shown.

# References


(1) Hestand, N. J.; Spano, F. C. Molecular aggregate photophysics beyond the Kasha model: novel design principles for organic materials. *Acc. Chem. Res.* **2017**, *50*, 341–350.

(2) Hestand, N. J.; Spano, F. C. Expanded theory of H-and J-molecular aggregates: the effects of vibronic coupling and intermolecular charge transfer. *Chem. Rev.* **2018**, *118*, 7069–7163.

(3) Spano, F. C. The spectral signatures of Frenkel polarons in H-and J-aggregates. *Acc. Chem. Res.* **2010**, *43*, 429–439.

(4) Pochas, C. M.; Spano, F. C. New insights on the nature of two-dimensional polarons in semiconducting polymers: Infrared absorption in poly (3-hexylthiophene). *J. Chem. Phys.* **2014**, *140*, 244902.

(5) Ghosh, R.; Pochas, C. M.; Spano, F. C. Polaron delocalization in conjugated polymer films. *J. Phys. Chem. C* **2016**, *120*, 11394–11406.

(6) Ghosh, R.; Chew, A. R.; Onorato, J.; Pakhnyuk, V.; Luscombe, C. K.; Salleo, A.; Spano, F. C. Spectral signatures and spatial coherence of bound and unbound polarons in p3ht films: Theory versus experiment. *J. Phys. Chem. C* **2018**, *122*, 18048–18060.

(7) Ghosh, R.; Luscombe, C. K.; Hambsch, M.; Mannsfeld, S. C.; Salleo, A.; Spano, F. C. Anisotropic polaron delocalization in conjugated homopolymers and donor–acceptor copolymers. *Chem. Mater.* **2019**, *31*, 7033–7045.

(8) Ghosh, R.; Spano, F. C. Excitons and Polarons in Organic Materials. *Acc. Chem. Res.* **2020**, *53*, 2201–2211.

(9) Spano, F. C. Modeling disorder in polymer aggregates: The optical spectroscopy of regioregular poly (3-hexylthiophene) thin films. *J. Chem. Phys.* **2005**, *122*, 234701.

(10) Spano, F. C. Excitons in conjugated oligomer aggregates, films, and crystals. *Annu. Rev. Phys. Chem.* **2006**, *57*, 217–243.

(11) Chew, A. R.; Ghosh, R.; Shang, Z.; Spano, F. C.; Salleo, A. Sequential doping reveals the importance of amorphous chain rigidity in charge transport of semi-crystalline polymers. *J. Phys. Chem. Lett.* **2017**, *8*, 4974–4980.

(12) Scholes, D. T.; Yee, P. Y.; Lindemuth, J. R.; Kang, H.; Onorato, J.; Ghosh, R.; Luscombe, C. K.; Spano, F. C.; Tolbert, S. H.; Schwartz, B. J. The Effects of Crystallinity on Charge Transport and the Structure of Sequentially Processed F4TCNQ-Doped Conjugated Polymer Films. *Adv. Funct. Mater.* **2017**, *27*, 1702654.

(13) Chew, A. R.; Ghosh, R.; Pakhnyuk, V.; Onorato, J.; Davidson, E. C.; Segalman, R. A.; Luscombe, C. K.; Spano, F. C.; Salleo, A. Unraveling the effect of conformational and electronic disorder in the charge transport processes of semiconducting polymers. *Adv. Funct. Mater.* **2018**, *28*, 1804142.

(14) Aubry, T. J.; Axtell, J. C.; Basile, V. M.; Winchell, K.; Lindemuth, J. R.; Porter, T. M.; Liu, J.-Y.; Alexandrova, A. N.; Kubiak, C. P.; Tolbert, S. H., et al. Dodecaborane-Based Dopants Designed to Shield Anion Electrostatics Lead to Increased Carrier Mobility in a Doped Conjugated Polymer. *Adv. Mater.* **2019**, *31*, 1805647.

(15) Aubry, T. J.; Winchell, K.; Salamat, C. Z.; Basile, V. M.; Lindemuth, J. R.; Stauber, J. M.; Axtell, J. C.; Kubena, R. M.; Phan, M. D.; Bird, M. J., et al. Tunable Dopants with Intrinsic Counterion Separation Reveal the Effects of Electron Affinity on Dopant Intercalation and Free Carrier Production in Sequentially Doped Conjugated Polymer Films. *Adv. Funct. Mater.* **2020**, 2001800.

(16) Voss, M. G.; Scholes, D. T.; Challa, J. R.; Schwartz, B. J. Ultrafast transient absorption spectroscopy of doped P3HT films: distinguishing free and trapped polarons. *Faraday Discuss.* **2019**, *216*, 339–362.

(17) Kahmann, S.; Fazzi, D.; Matt, G. J.; Thiel, W.; Loi, M. A.; Brabec, C. J. Polarons in narrow band gap polymers probed over the entire infrared range: a joint experimental and theoretical investigation. *J. Phys. Chem. Lett.* **2016**, *7*, 4438–4444.

(18) Kahmann, S.; Loi, M. A.; Brabec, C. J. Delocalisation softens polaron electronic transitions and vibrational modes in conjugated polymers. *J. Mater. Chem. C* **2018**, *6*, 6008–6013.

(19) Yu, H.; Wang, D. Metal-free magnetism in chemically doped covalent organic frameworks. *J. Am. Chem. Soc.* **2020**, *142*, 11013–11021.